Electrical Impedance Guides Electrode Array in Cochlear Implantation using Machine Learning and Robotic Feeder

Nauman **Hafeez**[a,*], Xinli **Du**[a], Nikolaos **Boulgouris**[a], Philip **Begg**[b], Richard **Irving**[b], Chris **Coulson**[b] and Guillaume **Tourrel**[c]

[a]*Institute of Environment, Health and Societies, Brunel University, UB8 3PH, London, UK*
[b]*University Hospitals Birmingham NHS Foundation Trust, B15 2GW, Birmingham, UK*
[c]*Oticon Medical Neurelec Inc., 06220, Vallauris, France*

ARTICLE INFO

ABSTRACT

Cochlear Implant provides an electronic substitute for hearing to severely or profoundly deaf patients. However, postoperative hearing outcomes significantly depend on the proper placement of electrode array (EA) into scala tympani (ST) during cochlear implant surgery. Due to limited intra-operative methods to access array placement, the objective of the current study was to evaluate the relationship between EA complex impedance and different insertion trajectories in a plastic ST model. A prototype system was designed to measure bipolar complex impedance (magnitude and phase) and its resistive and reactive components of electrodes. A 3-DoF actuation system was used as an insertion feeder. 137 insertions were performed from 3 different directions at a speed of 0.08 mm/s. Complex impedance data of 8 electrode pairs were sequentially recorded in each experiment. Machine learning algorithms were employed to classify both the full and partial insertion lengths. Support Vector Machine (SVM) gave the highest 97.1% accuracy for full insertion. When a real-time prediction was tested, Shallow Neural Network (SNN) model performed better than other algorithms using partial insertion data. The highest accuracy was found at 86.1% when 4 time samples and 2 apical electrode pairs were used. Direction prediction using partial data has the potential of online control of the insertion feeder for better EA placement. Accessing the position of the electrode array during the insertion has the potential to optimize its intraoperative placement that will result in improved hearing outcomes.

1. Introduction

A cochlear implant (CI) is an electronic device that provides restoration of sensorineural hearing in completely or partially deaf patients (Zeng et al., 2008). Among its other parts, a thin flimsy electrode array (EA) is inserted into the inner ear to directly stimulate the hearing nerve fibers. After the expansion of CI candidacy criteria in several countries (Vickers et al., 2016), it is fundamentally important to preserve residual hearing during the surgery to avoid variability in speech outcomes after the implantation (Gifford et al., 2013).

It is widely accepted that residual hearing loss is due to trauma-induced during the surgery (Eshraghi et al., 2006). The induced trauma could be due to different reasons (e.g., EA touching the inner ear walls, array tip foldover, and basilar membrane puncture) and can cause more or less damage according to the performed insertion (Hoskison et al., 2017). The current insertion method of EA does not provide any feedback to the the the surgeons with respect to the insertion trajectory and actions of electrode insertion. Insertion failure can only be assessed postoperatively through CT scan (Aziz et al., 2019) or if the surgeon takes intraoperative x-rays (Appachi et al., 2018). Scientists also found correlations between residual hearing loss and intraoperative Electrocochleography (ECochG) (Dalbert et al., 2016; Pfiffner et al., 2018). Correcting the insertion failure is itself a traumatic procedure, where the surgeon must remove the implant and re-implant it.

The variability in speech outcome is mainly due to positioning of the CI among other factors such as biography and audiology, EA design, surgical method and the magnitude of tone-evoked responses (Finley et al., 2008). There are three objectives of EA insertion for better hearing outcomes: (1) stimulate as much of the frequency range of the cochlear nerve as possible, (2) achieve close proximity to the modiolus wall (which contains the auditory nerve) to ensure greater operating efficiency and (3) to preserve residual hearing by preserving inner ear structure. To achieve

---

*Corresponding author
✉ nauman.hafeez@brunel.ac.uk (N. Hafeez)
ORCID(s): 0000-0003-2162-9054 (N. Hafeez)

an atraumatic insertion, the insertssion force should be limited due to sensitive inner ear anatomy which is beyond the sensitivity of human hand for such small forces and ultimately different forms of damage is expected. For these reasons, automated insertion tools are investigated with insertion speed and angle control, and force sensing capabilities. (Rau et al., 2011; Schurzig et al., 2010; Miroir et al., 2012; De Seta et al., 2017) used different types of electrode arrays, insertion techniques, scala tympani (ST) friction, and insertion speed to evaluate the impact of insertion forces. The limitation of force sensing method is its inability to measure local insertion forces across different sections of the EA. It can, however, be used to measure overall contact force during insertion, which may not be useful for EA localization. These types of force measurements can be useful when comparing certain types of EAs and different insertion techniques.

All the cochlear implant systems have a built-in impedance measurement mechanism to check the functioning of electrodes after the implantation. Impedance measurements and tomography have been employed in various biomedical areas. The first real-time impedance measurement system during array insertion ex-vivo was developed by Tan et al. (Tan et al., 2013). Both monopolar and bipolar impedance measurements were taken during insertion with advance off stylet (AOS) technique to observe impedance change after stylet removal. A correlation between impedance values and intra-cochlear array position was also seen where high impedance values observed near the cochlear walls. The same approach was taken by Pile et. al. (Pile et al., 2017) to also see the effect of different insertion techniques (Standard Insertion Technique (SIT) and AOS) on impedance change during insertion. The relationship between the impedance value and proximity was attributed to the amount of fluid between the EA and the modiolar wall at a specific contact. There was a clear separation between impedance measurements of two techniques where impedances during AOS insertion were higher than SIT.

Although all CI systems have built-in impedance capabilities, none of them has clinically used the complex impedance yet. In current CI systems, only impedance magnitude is measured and analyzed clinically. However, the interface between the CI electrode and its surroundings (perilymph fluid and tissues) is also important both in terms of postoperative speech outcomes as well as during the surgery. This interface is linked to components of overall impedance. Vanpoucke et al. (Vanpoucke et al., 2004) proposed a comprehensive electrical equivalent model of the implanted cochlear prosthesis to better understand the spread of neural excitation. The proposed network was based on monopolar intracochlear potential measurements and composed of two components; electrode-electrolyte interface impedance and tissue impedance. Interface impedance of an electrode contact was based on the circuit for a simple redox reaction (Schmickler et al., 2010). It consists of Warburg capacitance in parallel with charge transfer resistance and a series bulk resistance. Tissue impedance was modelled as a simplified version of lumped parameter model proposed by Suesserman(Suesserman et al., 1993) but a purely resistive model was adopted. A ladder network of segments of longitudinal and transversal resistors was modeled where the former represents a node connection to adjacent segments and the latter represents a connection to the ground node. Numerical methods were used to estimate the impedance equivalent model parameters.

Tykocinski (Tykocinski et al., 2005) proposed a model similar to Vanpoucke's interface impedance model, but regarded tissue impedance as part of access resistance. Equivalent model parameters (access resistance (R_a), polarization capacitance (C_p) and resistance (R_p)) were estimated using graphical methods instead by using voltage response to biphasic current pulse. On the same line, Newbold et al. (Newbold et al., 2010) considered the same electrode-tissue model to relate impedance changes with cell growth and protein absorption after cochlear implantation. Giardina et al. (Giardina et al., 2017) later used Tykocinski's method to correlate these component measurements with the proximity of the electrode array to the inner wall during the insertion of perimodiolar EA by using a linear regression model. The monopolar impedance measurement technique is used where overall impedance increased (R_a and R_p increased whereas C_p decreased) with respect to depth and proximity to the inner wall in a plastic ST model. The change in these values was attributed to the electrode-saline interface and surrounding structure.

Mesnildrey et al (Mesnildrey et al., 2019) adopted a rather complex equivalent circuit based on these previous studies (Duan et al., 2004; Franks et al., 2005) to estimate access resistance. The equivalent circuit compromised of blocking capacitor, parallel combination of constant phase element and Faradic resistance, access resistance, and parasitic capacitance. However, Faradic resistance was removed from the analysis as it yielded very high estimation in vitro. While comprehensively exploring electrode-tissue characteristics, Di Lella et al. (Di Lella et al., 2020) adopted the existing equivalent model as presented in (Vanpoucke et al., 2004; Tykocinski et al., 2005; Newbold et al., 2010), however, the study concluded that R_a and C_p are the most important components of the equivalent model. R_p can be ignored due to negligible variation of total impedance over a wide range of its values. For regular postoperative assessment of CI recipients, Di Lella et al (Di Lella et al., 2019) devised a remote method to measure impedance and its

components. However, it is only used for post-operative rehabilitation purposes. In the above works, such assessment has not included the impedance phase in the evaluation. Furtherm it was carried out in such a way that it does not allow real-time monitoring of the insertion process.

Impedance measurements of electrode contacts are influenced by their position in the cochlea (Tan et al. (2013); Pile et al. (2017); Giardina et al. (2017)). Based on this assumption, Aebischer et al. (Aebischer et al., 2020) proposed an approach to estimate insertion depth of EA using tissue impedance. Tissue impedances were extrapolated from trans-impedance recording data of 20 cochlear implanted subjects and were correlated with EA angular and linear insertion depth estimated from postoperative CT images. For this purpose, an impedance equivalent model was adopted from (Vanpoucke et al. (2004)), where total electrode impedance Z_e is a combination of interface impedance Z_i and tissue resistance R_t ($Z_e = Z_i + R_t$). The study found out that extrapolated tissue resistances from impedance matrix were higher for deeper electrodes. This could be attributed to the varied anatomy and length of the return path.

Robotic cochlear implantation has been tested ex-vivo to monitor the EA insertion avoid trauma. Force sensors are employed to see the effect of forces on trauma-induced during the array placement (Kaufmann et al., 2020). This is attributed to the fact that the surgeon performs insertion by hand (potential tremor) without any visualization of the inner ear and limited sensory feedback. A robotic insertion system with precise speed, trajectory, and position control can be a solution. To measure action and reaction forces, two force sensors are used. One sensor on the insertion tool and the other below the cochlea, which not only increases the cost of the system but is also impractical because it requires the use of a force sensor under the patient's head.

The focus of this study is to measure impedance magnitude ($|Z|$), phase (θ), impedance real (resistance, R), and imaginary parts (capacitive reactance, X_c) during EA insertion and applying machine learning algorithms to classify insertions (both full and partial) based on their trajectories. This method could be used for real-time detection of EA proximity to the ST walls based on complex impedance features. Our hypothesis is that insertion at different trajectories will have different force profiles and hence different impedance changes. This method will be combined with the robotic CI insertion approach to provide an automatic atraumatic CI operation.

2. Methodology

2.1. Experimental Setup

For this study, Oticon Medical's soft and straight EVO® electrode array was used with an insertion length of 25 mm and an active length of 24 mm (left side of Fig. 2). It is a flexible array with a smooth silicone surface carrying 20 micro- machined platinum-iridium electrodes. The electrodes are numbered from E1 to E20 where the former is the basal and the latter is apical electrode.
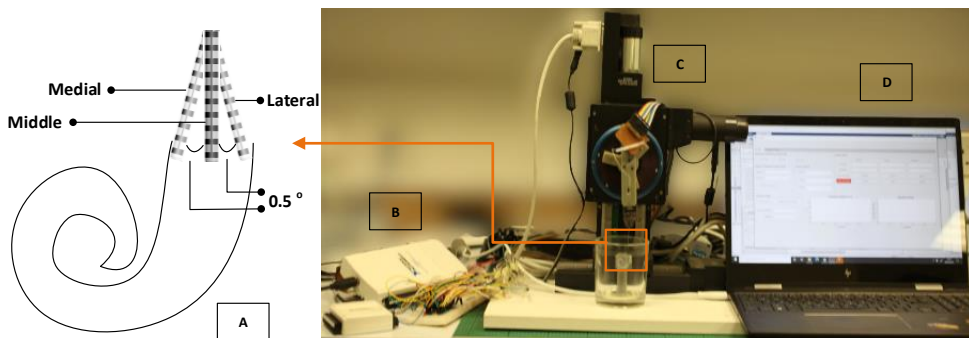

Figure 1: Experimental Setup., (A) Insertion from three different directions (medial, middle and lateral) of ST, (B) Impedance meter using DAQ devices and breadboard to house circuit and multiplexers,(C)Actuation system with electrode array feeder and ST plastic model, (D) Laptop with MATLAB GUI to control both impedance meter and actuation system. (Hafeez et al., 2019)

A 2:1 scaled-up plastic 2D cochlear model was used which was filled with the saline solution of 0.9% concentration as an alternative to perilymph fluid in the human ST. For consistent insertion trials, an automated system was used that

has two translational stages and one rotational stage. The insertion speed and angle can be controlled by a custom MATLAB® 2020a (Mathworks, Inc., Natick, MA USA) GUI-based application. Physik Instrumente (PI) (Waldbronn, Germany) M-404 and M-061 devices were used for translational and rotational stages respectively and PI's C-863 servo controllers as drivers of these stages (Fig. 1(C)).

Our impedance model is based on Tykocinski (Tykocinski et al., 2005), and consists of three components, 1) resistance between electrodes due to bulk medium (saline), 2) polarization resistance and 3) capacitive reactance due to electrode-electrolyte interface. Components (2) and (3) combined are called polarization impedance and can be modeled as a parallel circuit with (1) in series with them. According to this model, we not only need to measure impedance magnitude but also the phase, and impedance resistive and reactive components to fully comprehend the model and use these features for prediction. For this, a system for complex impedance measurement was developed using National Instrument (NI) (Austin, TX USA) Data Acquisition Device (DAQ) devices and a simple voltage divider circuit. All analog and digital signals were generated and read by the DAQ devices and these devices were controlled by custom software written in MATLAB ® (Fig. 2). The voltage divider circuit was constructed with a known resistance (R) of 3.3Ω and electrode pair (EP) as its series component. A sinusoidal voltage signal V_{in} of 1V (p-p) with 1 kHz frequency was applied to the circuit and voltage across known resistance (V_R) and EP (V_{EP}) were measured by the DAQ device. Voltage input signal to the circuit V_{in} was generated by DAQ's voltage output port A_o and measured voltages (V_R and V_{EP}) were read by DAQ's input ports A_{i1} and A_{i2} respectively. Current I through the circuit can be calculated with (1)

$$I = \frac{V_R}{R} \tag{1}$$

Impedance is a complex quantity that possesses both magnitude and phase and can be given as (2). Impedance
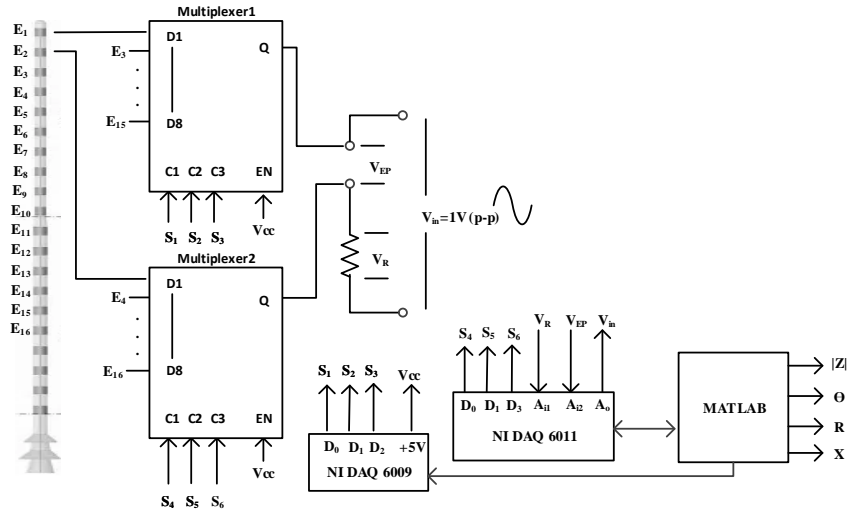

Figure 2: Impedance measurement system. Setup chain - electrodes ($E_1 - E_{16}$) are connected to series circuit via 2 multiplexers, circuit is connected to the DAQ devices that are interfaced with MATLAB running on windows laptop. $V_{in} = 1V(p-p)$ is the input applied to the series circuit, V_R and V_{EP} are measured to calculate outputs $|Z|$, Θ, R and X of an EP. A_o and A_{Ai1}, A_{Ai2} are DAQ's analog output and input ports respectively. $D_0 - D_2$ are digital output ports of DAQ devices to generate digital signals $S_1 - S_6$ for multiplexers' select lines $C1 - C3$ to scan EPs. $D1 - D8$ are multiplexer input ports and Q is the output port. 5V Vcc signal is applied to multiplexer enable ports.

magnitude is the opposition to the current when an AC voltage is applied. Bipolar impedance magnitude $|Z|$ of

selected electrode pair is just voltage across electrode pair divided by the current through it as in (3)

$$Z = |Z|e^{j\theta} \tag{2}$$

$$|Z| = \frac{V_{EP}}{I} \tag{3}$$

The impedance phase ($arg(Z)$ or θ) gives information about the type and amount of reactance in overall impedance. It is calculated by taking the phase difference between voltage and current as in (4)

$$\angle\theta = \angle\theta_{V_{EP}} - \angle\theta_I \tag{4}$$

As we are considering an equivalent circuit of electrode array within the ST, where polarization element (a resistor in parallel with a capacitor) is in series with a resistor, it is important to calculate resistive and capacitive reactance as in (5) and (6). According to a study conducted by Di Lella et al. (Di Lella et al., 2020), there is a negligible variation of polarization impedance due to polarization resistance change. Therefore, polarization resistance is ignored in our analysis. Access resistance is represented by R and reactance due to polarization capacitance is represented as X.

$$R = |Z|cos\theta \tag{5}$$

$$X = |Z|sin\theta \tag{6}$$

Two 74HC4051 8x1 multiplexers were used to sequentially switch from one pair to another and measure bipolar complex impedance between different electrode pairs. Each multiplexer has 8 data inputs D1-D8, 3 select lines C1-C3, and enable input EN and an output Q. Electrode contacts were connected to data input pins of multiplexers such that an electrode contact was selected by each multiplexer to make a pair. Multiplexer1 and multiplexer2 were controlled by 3 digital output signals S1-S3 generated by DAQ6009 device digital output ports ($D_0 - D_2$) and S4-S6 generated by DAQ6011 digital output ports ($D_0 - D_2$), respectively. These select lines vary from 000-111 as digital signals to select appropriate contact to form an electrode pair for impedance measurement. When an electrode contact was selected, a connection was established between the contact and the output Q. The enable signal EN was connected to +5V Vcc signal from the DAQ6009 device to activate the multiplexers. When multiplexers were enabled and an EP was selected, signals were applied and read from series circuit to measure outputs |Z|, Θ, R and X according to the above equations.

The limitation of above method is its use with commercially available cochlear implants. This method would require an intermediary adapter to be connected to the electrode array or an update to the CI software for impedance measurement. One such work has been done by (Di Lella et al., 2020) where a custom software has been used to measure impedance sub-components using mathematical formulae and also experimentally validated.

2.2. Study Design and Data Assembly

The electrode array was inserted from three different angles (medial, middle, and lateral) where the middle position was centered at the plastic model, medial and lateral at 0.5° to either side from the center towards modiolar and lateral walls respectively as shown in (Fig. 1, A). Initially, the electrode array was out of saline (and out of ST model) except first pair EP1 (E1-E2). A high impedance measurement was recorded if a pair was out of saline that depicted an open circuit scenario. The electrode array was inserted into the ST model for 25 mm at a speed of 0.08 mm/s by moving the vertical linear actuator (EA is placed on it with a holder). Recordings of 8 electrode pairs (EP1:E1-E2, EP2:E3-E4, ... EP8:E15-E16) were taken with a sampling time of 1.5s. Therefore, each pair has 25 samples during complete insertion (1 sample/pair/~mm).

Electrode array was inserted for 25mm in ST model 137 times from three different directions; 41 times each from left (medial) direction and right (lateral) directions and 55 times from the middle of ST model. For each insertion, two

features ($|Z|$, θ) of an electrode pair were recorded sequentially during insertion and impedance real and imaginary parts were calculated from its magnitude and phase. During one complete insertion, each electrode pair records a vector $\mathbf{P}^{(i)} = [\mathbf{Z}^{(i)}, \mathbf{\Theta}^{(i)}, \mathbf{R}^{(i)}, \mathbf{X}^{(i)}]$ containing m samples of impedence magnitude $\mathbf{Z}^{(i)} = [|Z|_1^{(i)}, |Z|_2^{(i)}, \ldots, |Z|_m^{(i)}]$, phase $\mathbf{\Theta}^{(i)} = [\theta_1^{(i)}, \theta_2^{(i)}, \ldots, \theta_m^{(i)}]$, and both real and imaginary parts of the impedence given by $\mathbf{R}^{(i)} = [R_1^{(i)}, R_2^{(i)}, \ldots, R_m^{(i)}]$ and $\mathbf{X}^{(i)} = [X_1^{(i)}, X_2^{(i)}, \ldots, X_m^{(i)}]$ respectively. Here $m = 25 - 2(i-1)$ for all $i \in \{1, 2 \ldots, 8\}$. The reason for decrease in samples in subsequent pairs was discarding high impedance measurements when a pair was out of saline solution during the insertion process.

2.3. Classification Algorithms

A time-series T is a sequence of measurements of size m taken over a period at regular intervals where $T = (t_1, t_2, \ldots, t_m)$. In machine learning, time series classification refers to the process of learning meaningful information from temporally ordered data and classifying each data point into a class. This has led to it being studied extensively under various machine learning algorithms (Kalman et al., 1960; Vapnik, 1995; Vapnik et al., 1998; Cristianini et al., 2000).

Three algorithms were used for the prediction of different EA trajectories. 1) Support Vector Machines (SVM) were initially designed as discriminative functions and were mainly used for large margin classification. Simply put, given a set of training examples, the SVM classifier learns the position of its support vectors and then subsequently the optimal hyperplane to categorize unseen samples. Owing to their impressive generalization ability, SVMs have been extensively studied to solve a number of classification tasks (see e.g. (Vapnik, 1995; Boser et al., 1992; Schiilkop et al., 1995)). 2) k-Nearest Neighbor (kNN) classifier is a fairly simple and straightforward supervised learning algorithm that classifies a data point based on how its neighbors are classified. kNN algorithm is based on feature similarity, that is, choosing the right k (number of neighbors) value is important for better accuracy. Another parameter is the distance measure that induces the relationship between neighbors (Cover et al., 1967), for example, Euclidean distance, Dynamic Time Warping (DTW), Manhatten distance, etc. 3) Artificial Neural Networks (ANN) are complex computational data-driven models. An ANN is composed of simple computational nodes, called neurons, typically arranged in the form of layers. Each layer performs a simple linear transformation on the incoming data, followed by a pointwise non-linear function (Livingstone, 2008). A Shallow Neural Network (SNN) is an ANN with 1 or 2 hidden layers and will be used in this work.

2.4. Workflow

The workflow for this experimental study is given in Fig. (3). It involved the classification of three different classes using machine learning algorithms. Starting off with data collection of electrical features of electrodes during insertion experiments. Dataset assembling and visualization were the next steps to set up data in a certain manner and visualize it for analysis. Preprocessing is one of the important steps (García et al., 2015) which includes, in our case, excluding any high impedance value or averaging out any high impedance/short circuit value. We opted for excluding all high impedance values. There are two options before dividing the dataset for training and testing a machine learning model; either using the normalized/standardized raw data or extract the features from the time series data and select the most discriminant features. The former method was adopted as it reduces the time to predict on run time. After splitting the dataset into 70/30 train and test sets, The training dataset was standardized by subtracting the mean and dividing by the standard deviation. The mean and variance computed from the training set were then used to transform the test data. Each sample of a dataset was flattened as a vector. After this, machine learning models (kNN/SVM/SNN) were trained and tested. Their accuracies were compared, and an optimal model was selected for further validation and utilization as an online predictor. All machine learning models were implemented using python's sklearn library (Pedregosa et al., 2011).

From 137 full insertion data examples, several datasets were created from different combinations of electrode pairs utilizing four electrical properties of electrodes to analyze their significance in classification. Three different classifiers (SNN, KNN, and SVM) were evaluated on different datasets based on features and the number of EPs. For SNN, we used a multilevel perceptron (MLP) with two hidden layers of size 100 and 10, respectively, and finally a classification layer with 3 neurons. The hidden layers had an associated non-linearity of rectified linear units (ReLU). A softmax layer was used to convert the output of the MLP into probabilities of the respective classes. The network was trained for 1000 epochs using an Adam optimizer at a learning rate of 0.001. For SVM, Radial Basis Function(RBF) kernel function was used to train the data and Dynamic Time Wrapping (DTW) was used as a distance metric and 5 number
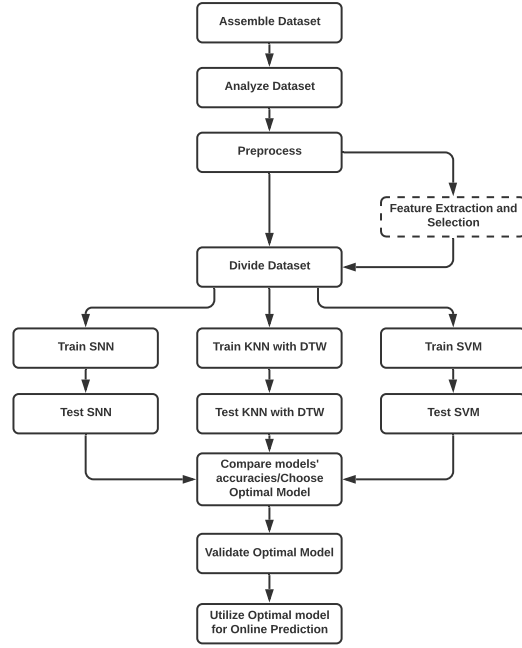
Figure 3: Workflow for classification

of neighbors for the kNN classifier model. Five runs of each classification set were carried out and average accuracy was measured.

For the short-term information of electrode array direction during the insertion, we need to perform classification on short subsequences of the full insertion data . Therefore, it could be used on run-time during EA insertion. The time-series sequence of the data was divided into subsequences with respect to the length of insertion in terms of time samples. The ideal scenario is to predict the insertion direction as early as possible with reasonable accuracy. Classification algorithms were trained and tested on these subsequences to predict EA insertion direction. A subsequence of length n of time series T is $T(i, n) = (t_i, t_{i+1}, \ldots, t_{i+n-1})$, where $1 \leq i \leq m - n + 1$ where m is the size of complete time series. Each full insertion sample was divided into subsequences of different time samples and classification accuracies were compared to different temporal data at different insertion depths. The minimum time samples tested were three for each feature and the maximum was eight in the increasing order. A maximum time sample of eight was chosen because four EPs were inserted during that time and it's when full insertion data gave maximum accuracy.

2.5. Evaluation Criteria

A confusion matrix was obtained for each set of data assembly (in terms of the number of electrode pairs used) and classifier utilized. From this matrix, it is possible to obtain the counts of true positive (TP), true negative (TN), false positive (FP) and false negative (FN) cases. For multi-class classification, these values are calculated for each class label (insertion direction) from our C_{NxN} confusion matrix as follows. The rows in confusion matrix represent actual class labels i and columns depict predicted labels j. In the present study, $i, j = \{left, middle, right\} \equiv \{1, 2, 3\}$. The following definitions of TP, TN, FP and FN apply to a given class label i

$$TP = C_{ii} \tag{7}$$

$$FP = \sum_{j=1}^{N} C_{ji} - Cii \tag{8}$$

$$FN = \sum_{j=1}^{N} C_{ij} - Cii \tag{9}$$

$$TN = \sum_{i=1}^{N} \sum_{j=1}^{N} C_{ij} - (TP + FP + FN) \tag{10}$$

From the above values, we have obtained accuracy performance measure as follows

$$Accuracy = \frac{TP + TN}{TP + FP + FN + TN} \tag{11}$$

3. Results

3.1. Dataset Visualization

Figure (4) shows line plots of 8 electrode pairs covering 4 features ($|Z|, \theta, R, X$) and three insertions trajectories (medial, middle, lateral). These plots are the average of the respective class samples with their standard deviation. Each row presents a feature and each column presents an insertion trajectory. The vertical axis of each plot is the feature value and insertion time is at the horizontal axis.

When EA is inserted from the middle, it does not touch any wall and remains in the middle of the structure until it touches the lateral wall after 15 mm insertion. After that, it slides along the lateral wall for the rest of the insertion. It can be seen that impedance magnitude increases as it touches the lateral wall and slides along with it due to force exerted on EA and else due to the proximity of electrodes to the plastic, which is a high impedance material. The impedance phase is becoming less negative during this period which exhibits less capacitive behavior. It may be due to disturbance in the electrochemical reaction between electrode and saline solution when it hits the lateral wall and slides along with it. When EA is inserted from the medial direction, EA slides along the modiolar wall and touches the lateral wall when the wall starts to curve. On the other hand, EA slides along the lateral wall during the lateral direction insertion and gets an impact when curving along the wall. Data visualization was carried out using Python's seaborn library (Waskom et al., 2017).

3.2. Full Insertion Classification

The objective is to classify which trajectory EA is inserted from using full insertion data of three different trajectories. Impedance magnitude, phase, resistance, and reactance values were measured of eight electrode pairs for 137 insertions. Out of those measurements, EA was inserted 41 times each from the medial and lateral direction and 55 times from the middle of the ST model. Table 1 presents test accuracies for three classifiers with different combinations of electrode pairs where EP1 is the most apical pair. For example, row 4 represents a dataset compromising of four feature time series of the first four electrode pairs (EP-1,2,3 and 4) and test accuracies of three machine learning (ML) models are presented when trained and tested on the said dataset. The last row presents the test set accuracies when all 8 electrode pairs are considered in the modeling. It is evident from the test accuracies of the three classifiers, higher test accuracy was achieved when we used four electrode pairs. It is also observed that a single electrode could also have high predictive information, for example, the first-row accuracy results where only the first pair was used. Relatively high accuracy of 94.2% is achieved using SNN. Two ML models (SNN and SVM) gave higher than 90% accuracy to predict three classes (Left, middle, and right direction insertions) except on one occasion considering all selection of pairs. SNN and SVM performed better than KNN for most of the EP data combinations. Overall SVM model gave the highest accuracy of 97.1% when we used four electrode pairs. With the same EP combination, SNN gave a test accuracy of 92.3%.

3.3. Sub-sequence classification

Although high accuracy results are achieved to predict different insertion trajectories using complete insertion measurement data, it is important to know how well the selected models predict on different subsequence datasets.
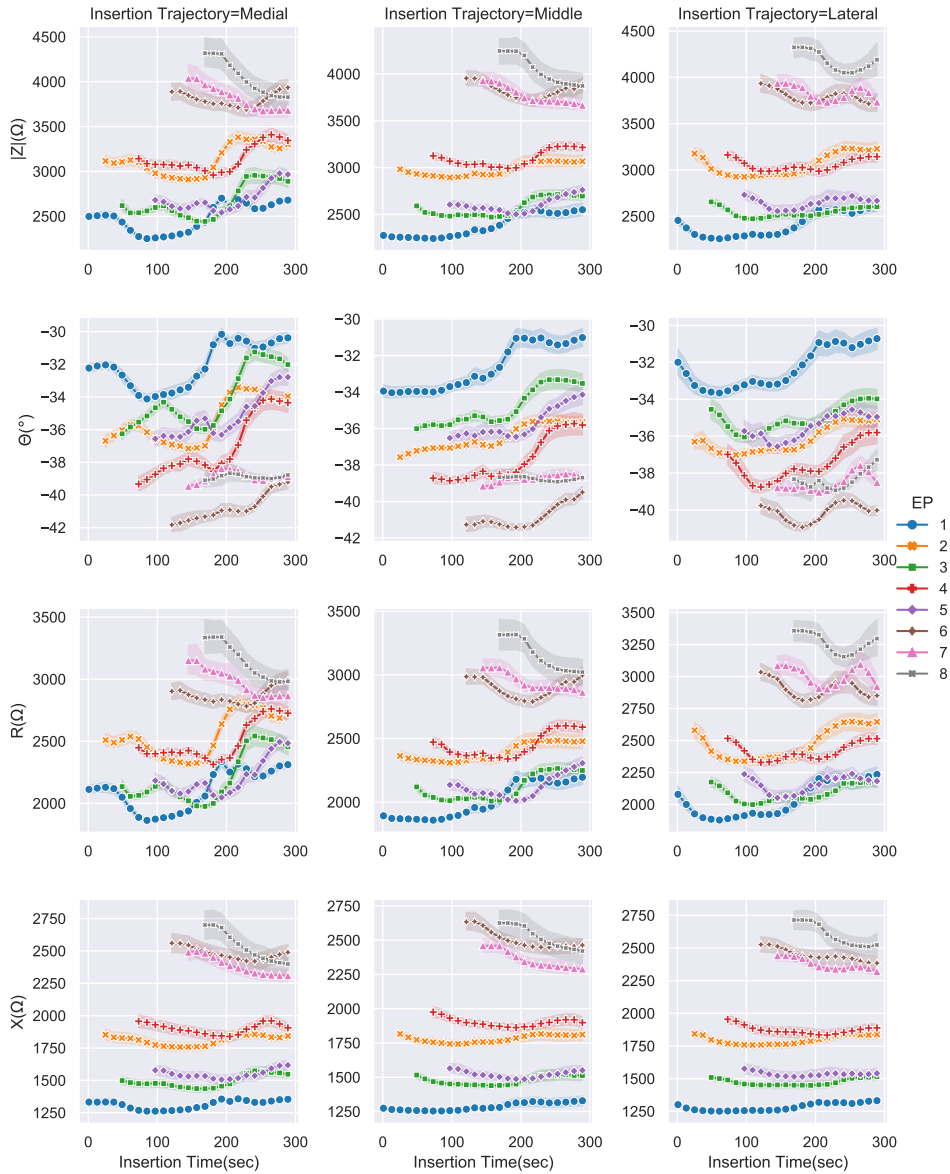
Figure 4: Complex impedance of eight electrode pairs. Rows in the overall figure represent features (From top to bottom: Impedance magnitude (Z(Ω)), phase (Θ(°)), resistance (R(Ω)), reactance (X(Ω)). Columns represent insertion trajectory (From left to right: Medial-Middle-Lateral). High Impedance values are ignored in respective electrode pair's plot.

The first column of Table 2 presents different time samples combination to form subsequences and the other three columns depict test accuracies at three ML models. With these subsequences, SNN overall gave the highest accuracy and SVM came in second. The highest accuracy was achieved (93.8%) when time samples 2-8 of each feature and relevant electrode pairs (which are inside the saline-filled model) were trained and tested. However, it takes time to wait for eight-time samples before we know the insertion direction. The sweet spot is when 1-4 time samples were used and 86.1% accuracy is achieved. This could work well for online prediction of EA insertion direction and the actuation system could be utilized to correct the direction during run time based on the prediction.

Table 1
Classification test accuracies of full insertion data with 4 features to classify insertion direction/trajectory

	EP	Accuracy (%)		
		SNN	SVM	KNN
$|Z|, \theta, R, X$	1	94.2	90.9	88.0
	$1-2$	92.3	94.7	92.8
	$1-3$	90.4	91.9	92.8
	$1-4$	92.3	**97.1**	92.8
	$1-5$	93.3	94.7	85.7
	$1-6$	94.2	89.5	90.4
	$1-7$	92.8	93.3	88.0
	$1-8$	93.3	90.9	90.4

Table 2
Classification test accuracy achieved using various machine learning algorithms on $|Z|, \theta, R$, and X values using different sub-sequences

timesamples	Accuracy (%)		
	SNN	SVM	KNN
$1-3$	85.2	78.5	80.0
$1-4$	86.1	82.3	80.9
$1-5$	82.8	78.0	71.9
$1-6$	87.1	83.8	83.3
$1-7$	86.1	81.4	76.6
$1-8$	86.6	89.5	74.7
$2-4$	86.1	79.5	81.9
$2-5$	87.6	79.0	76.6
$2-6$	86.6	82.8	86.1
$2-7$	87.6	79.0	80.0
$2-8$	93.8	81.9	78.5
$3-5$	84.2	76.6	73.8
$3-6$	92.3	78.0	80.4
$3-7$	92.8	81.9	80.0
$3-8$	91.9	85.2	84.2
$4-6$	82.8	75.7	73.8
$4-7$	90.9	76.6	72.3
$4-8$	91.4	80.9	72.8
$5-7$	87.6	77.1	77.6
$5-8$	85.7	79.0	79.0

4. Discussion

It is important to insert EA atraumatically to avoid residual hearing loss, however, it is difficult to do so without the availability of sensory information inside the ST during the insertion process. Impedance variation during insertion from different trajectories could be due to the different force profiles. As electrical impedance has been used for catheter and biopsy needle guidance (Park et al., 2018; Münkler et al., 2020) by incorporating microelectrodes, we are presenting a system compromising of complex electrical impedance sensory system and automated feed control for EA insertion. This system records the complex bipolar impedance of eight electrode pairs sequentially during the automated insertion and detects the direction it is being inserted from using a machine learning algorithm. It is important because the cochlea is a black box when EA is inserted in it and the proposed system gives localized information about the EA during insertion.

Our models gave reasonable accuracy both for full and partial insertion data while using all four of the complex impedance features. For full insertion data, the SVM algorithm gave the highest accuracy whereas SNN gave the highest accuracy for partial insertion data. Due to the non-linear nature of the problem, the BRF kernel function was used in our SVM model as suggested in other studies (Wang et al., 2008, 2012). We observed that SVM slightly outperformed SNN in full insertion classification. It is difficult to pin point a reason, however, it could be due to better parameter selection, non linearity of the problem, and/or SVM's better ability to converge to global minimum and tolerance to the noise. In terms of number of electrode pairs used in the classification data, it has been found out that

test accuracy increased with their increasing numbers. Partial insertion classification results are important due to their applicability for online detection and correction of EA insertion process. Accuracy of partial insertion dataset could be increased by measuring more time samples in a given time and producing more data per mm of insertion. These models were tested on scaled raw data, however, feature extraction and selection technique was also employed using Python's TSFRESH package (Christ et al., 2018) to test the models but achieved almost similar results.

The angle of the cochlear approach or EA insertion trajectory has gained attention recently in the research community as it has been observed that certain trajectories are optimal for atraumatic insertion of electrode array (Topsakal et al., 2020; Morrel et al., 2020). Array insertion from certain angles effectively has different force profiles both on cochlea walls and basilar membrane which eventually leads to intra-cochlear trauma (Torres et al., 2017). Insertion trajectory also influence insertion depth (number of electrodes inserted successfully in the ST) of the electrode array. A poor trajectory could also lead to array translocation in to scala vestibuli (Torres et al., 2018). The ideal axis for the insertion is the centerline of the ST, however, it is not possible to insert from ideal axis due to facial canal position. For this, optimal axis has to be defined before the surgery to avoid facial canal. The mental representation of the optimal axis depends on the surgeon's experience in the manual surgery (Torres et al., 2016). Wimmer et al. (Wimmer et al., 2014) proposed a method to find this optimal trajectory using two planes (inplane and outplane angle) for robotic surgeries. However, this is a pre-operative method and there is no information of EA direction when its inside the ST. Our work is vital in this respect that it gives information about the EA insertion direction inside ST and it could also be used to adjust the direction during the insertion process with the robotic feed system in case it gets away from optimal path.

An important step to optimize the EA insertion process is the design of an automatic feeder system with an option of variable insertion speed adjustment. Such a system reduces the variability caused by the manual procedure in speed, tremor, and insertion duration. The proposed sensing system works best with such a robotic tool. The limitation of the feeder system we used is bulkiness and it might be difficult to attach to a robotic arm for easy maneuvering in the operating theatre. The second limitation is EA insertion duration due to the limitation of impedance meter sampling time. It is important to record at least 1 sample/EP/mm of insertion. However, lower insertion speed was associated with lower insertion trauma and better post-surgery hearing outcomes (Miroir et al., 2012; Kontorinis et al., 2011). Finally, it would be interesting to correlate complex impedance with the insertion forces and train the ML models to stop the insertion when a certain threshold exceeds to avoid intraoperative damage.

The presented work is a preliminary study where a scaled-up 2D plastic ST model was used. We may say, it is one of the limitations considering replicating the experiments in cadavers. The reason for using the scaled-up model was the easy visibility of EA in the model. Also, since the first cochlear turn is the major cause of trauma-induced (Zeng et al., 2008), we used the 2D model as there is a slight difference in 2D and 3D models with respect to the first turn. The authors intend to do further studies with a 3D real-sized cochlear model in the future. We believe due to more close contacts in a real size cochlea, our model may give similar or better results. The experiments were performed in a plastic model, while on the other hand in-vivo recordings introduce bones and tissue structures during insertion. These structures do tend to introduce variability (non-linear behavior) in the measurements, however, they may be more helpful in locating the directions/positions of the EA than the plastic model. The future direction is to test the system on temporal bones and cadaveric models.

It is understandable that all cochlear implants measure impedance differently (current stimulation first and then voltage measurement) than the proposed method and only measure impedance magnitude. Due to this reason, the system is not directly translational, however, we consider our system as a standalone robotic insertion platform with a novel sensing mechanism that requires access to the electrode contacts of CI to measure the proposed feature set during insertion to make a prediction. The extension to the proposed work is in pipeline where this system would be tested as a closed-loop feedback system for real-time prediction and correction of insertion trajectory, potentially to minimize the trauma.

One of the limitations of the proposed study is the dependence of bipolar impedance measurement on conductive fluid. Any measurement outside saline solution is a high impedance value and barely useful. There needs to be a mechanism for the automatic exclusion of such measurements from the feature set. There is another limitation in terms of variability in discriminative measurements due to different electrode arrays or measurement conditions which may limit the generalization of the machine learning algorithms. This limitation can be addressed by characterization and calibration of the implant prior to use. Lastly, the proposed work has used 3 trajectories which may not be representative of several other insertion possibilities. Further investigation needs to be done by incorporating additional trajectory variants, for example, similar to the work by Martins et al. (Martins et al., 2015) where they are accessing trauma when

EA is inserted from different round window quadrants. Nonetheless, the proposed work is a step forward towards more accurate predicted implantation which may also have application in other electrode implants.

5. Conclusion

Insertion trajectory is crucial for trauma-less insertion of the electrode array into the cochlea. It is also of vital importance that surgeons know of the EA directions once it's in the ST. This research focused on classifying EA insertion from three different angles/positions of the ST using machine learning algorithms. Firstly, classification algorithms were trained and tested on full insertion data where SVM performed (above 95% accuracy) better than SNN and kNN, however, comparable results were obtained with SNN. To make this system work online, models were tested on partial (time series segmented into sub-sequences) insertion data, SNN performed well on this occasion. A number of datasets with a different combination of electrode pairs were analyzed and found out we get better accuracies with a higher number of pairs. We believe that this system builds an excellent platform for better positioning and placement of electrode array in cochlear implantation.

Acknowledgments

Funding

Conflict of Interest

The authors declare no conflict of interest.

References

Aebischer, P., et al., 2020. Intraoperative impedance-based estimation of cochlear implant electrode array insertion depth. IEEE transactions on biomedical engineering 68, 545–555.

Appachi, et al., 2018. Utility of intraoperative imaging in cochlear implantation: A systematic review. The Laryngoscope 128, 1914–1921.

Aziz, A.E., et al., 2019. Radiological evaluation of inner ear trauma after cochlear implant surgery by cone beam ct (cbct). European Archives of Oto-Rhino-Laryngology 276, 2697–2703.

Boser, et al., 1992. A training algorithm for optimal margin classifiers, in: Proceedings of the fifth annual workshop on Computational learning theory, pp. 144–152.

Christ, et al., 2018. Time series feature extraction on basis of scalable hypothesis tests (tsfresh–a python package). Neurocomputing 307, 72–77.

Cover, et al., 1967. Nearest neighbor pattern classification. IEEE transactions on information theory 13, 21–27.

Cristianini, et al., 2000. An introduction to support vector machines and other kernel-based learning methods. Cambridge university press.

Dalbert, et al., 2016. Assessment of cochlear trauma during cochlear implantation using electrocochleography and cone beam computed tomography. Otology & Neurotology 37, 446–453.

De Seta, D., et al., 2017. Damage to inner ear structure during cochlear implantation: Correlation between insertion force and radio-histological findings in temporal bone specimens. Hearing research 344, 90–97.

Di Lella, F.A., et al., 2019. In vivo real-time remote cochlear implant capacitive impedance measurements: A glimpse into the implanted inner ear. Otology & Neurotology 40, S18–S22.

Di Lella, F.A., et al., 2020. Measuring the electrical status of the bionic ear. re-thinking the impedance in cochlear implants. Frontiers in Bioengineering and Biotechnology 8, 1095.

Duan, et al., 2004. A study of intra-cochlear electrodes and tissue interface by electrochemical impedance methods in vivo. Biomaterials 25, 3813–3828.

Eshraghi, et al., 2006. Cochlear implantation trauma and noise-induced hearing loss: Apoptosis and therapeutic strategies. The Anatomical Record Part A: Discoveries in Molecular, Cellular, and Evolutionary Biology: An Official Publication of the American Association of Anatomists 288, 473–481.

Finley, et al., 2008. Role of electrode placement as a contributor to variability in cochlear implant outcomes. Otology & neurotology: official publication of the American Otological Society, American Neurotology Society [and] European Academy of Otology and Neurotology 29, 920.

Franks, et al., 2005. Impedance characterization and modeling of electrodes for biomedical applications. IEEE Transactions on Biomedical Engineering 52, 1295–1302.

García, et al., 2015. Data preprocessing in data mining. Springer.

Giardina, et al., 2017. Impedance measures during in vitro cochlear implantation predict array positioning. IEEE Transactions on Biomedical Engineering 65, 327–335.

Gifford, et al., 2013. Cochlear implantation with hearing preservation yields significant benefit for speech recognition in complex listening environments. Ear and hearing 34, 413.

Hafeez, et al., 2019. Towards unblinding the surgeons: Complex electrical impedance for electrode array insertion guidance in cochlear implantation, in: Proceedings of the International Symposium on Auditory and Audiological Research, pp. 29–36.

Hoskison, et al., 2017. Systematic review: radiological and histological evidence of cochlear implant insertion trauma in adult patients. Cochlear Implants International 18, 192–197.

Kalman, et al., 1960. A new approach to linear filtering and prediction problems [j]. Journal of basic Engineering 82, 35–45.

Kaufmann, et al., 2020. Evaluation of insertion forces and cochlea trauma following robotics-assisted cochlear implant electrode array insertion. Otology & Neurotology 41, 631–638.

Kontorinis, et al., 2011. Impact of the insertion speed of cochlear implant electrodes on the insertion forces. Otology & neurotology 32, 565–570.

Livingstone, D.J., 2008. Artificial neural networks: methods and applications. Springer.

Martins, et al., 2015. Evaluation of intracochlear trauma caused by insertion of cochlear implant electrode arrays through different quadrants of the round window. BioMed research international 2015.

Mesnildrey, et al., 2019. Impedance measures for a better understanding of the electrical stimulation of the inner ear. Journal of neural engineering 16, 016023.

Miroir, et al., 2012. Friction force measurement during cochlear implant insertion: application to a force-controlled insertion tool design. Otology & neurotology 33, 1092–1100.

Morrel, et al., 2020. Custom mastoid-fitting templates to improve cochlear implant electrode insertion trajectory. International journal of computer assisted radiology and surgery .

Münkler, et al., 2020. Local impedance guides catheter ablation in patients with ventricular tachycardia. Journal of Cardiovascular Electrophysiology 31, 61–69.

Newbold, et al., 2010. Changes in biphasic electrode impedance with protein adsorption and cell growth. Journal of neural engineering 7, 056011.

Park, et al., 2018. Biopsy needle integrated with electrical impedance sensing microelectrode array towards real-time needle guidance and tissue discrimination. Scientific reports 8, 1–12.

Pedregosa, et al., 2011. Scikit-learn: Machine learning in python. the Journal of machine Learning research 12, 2825–2830.

Pfiffner, et al., 2018. Correlation between extracochlear electrocochleography responses during cochlear implantation and hearing preservation. Journal of Hearing Science 8.

Pile, et al., 2017. Detection of modiolar proximity through bipolar impedance measurements. The Laryngoscope 127, 1413–1419.

Rau, et al., 2011. Determination of the curling behavior of a preformed cochlear implant electrode array. International Journal of Computer Assisted Radiology and Surgery 6, 421–433. doi:10.1007/s11548-010-0520-x.

Schiilkop, et al., 1995. Extracting support data for a given task, in: Proceedings, First International Conference on Knowledge Discovery & Data Mining. AAAI Press, Menlo Park, CA, pp. 252–257.

Schmickler, et al., 2010. Interfacial electrochemistry. Springer Science & Business Media.

Schurzig, et al., 2010. Force of cochlear implant electrode insertion performed by a robotic insertion tool: comparison of traditional versus advance off-stylet techniques. Otology & neurotology: official publication of the American Otological Society, American Neurotology Society [and] European Academy of Otology and Neurotology 31, 1207.

Suesserman, et al., 1993. Lumped-parameter model for in vivo cochlear stimulation. IEEE transactions on biomedical engineering 40, 237–245.

Tan, et al., 2013. Real-time measurement of electrode impedance during intracochlear electrode insertion. The Laryngoscope 123, 1028–1032.

Topsakal, et al., 2020. Comparison of the surgical techniques and robotic techniques for cochlear implantation in terms of the trajectories toward the inner ear. The Journal of International Advanced Otology 16, 3.

Torres, et al., 2016. Variability of the mental representation of the cochlear anatomy during cochlear implantation. European Archives of Oto-Rhino-Laryngology 273, 2009–2018.

Torres, et al., 2017. Improvement of the insertion axis for cochlear implantation with a robot-based system. European Archives of Oto-Rhino-Laryngology 274, 715–721. doi:10.1007/s00405-016-4329-2.

Torres, et al., 2018. An Optimized Robot-Based Technique for Cochlear Implantation to Reduce Array Insertion Trauma. Otolaryngology - Head and Neck Surgery (United States) 159, 900–907. doi:10.1177/0194599818792232.

Tykocinski, et al., 2005. Measurement and analysis of access resistance and polarization impedance in cochlear implant recipients. Otology & Neurotology 26, 948–956.

Vanpoucke, et al., 2004. Identification of the impedance model of an implanted cochlear prosthesis from intracochlear potential measurements. IEEE Transactions on biomedical engineering 51, 2174–2183.

Vapnik, et al., 1998. Statistical learning theory wiley. New York 1, 624.

Vapnik, V.N., 1995. T he nature of statistical l earning t heory. New York: Springer2V erlag .

Vickers, et al., 2016. International survey of cochlear implant candidacy. Cochlear implants international 17, 36–41.

Wang, et al., 2008. Novel cell segmentation and online svm for cell cycle phase identification in automated microscopy. Bioinformatics 24, 94–101.

Wang, et al., 2012. A new automatic identification system of insect images at the order level. Knowledge-Based Systems 33, 102–110.

Waskom, et al., 2017. mwaskom/seaborn: v0. 8.1 (september 2017). Zenodo, doi 10.

Wimmer, et al., 2014. Semiautomatic cochleostomy target and insertion trajectory planning for minimally invasive cochlear implantation. BioMed research international 2014.

Zeng, et al., 2008. Cochlear implants: system design, integration, and evaluation. IEEE reviews in biomedical engineering 1, 115–142.